ACS APPLIED MATERIALS & INTERFACES

Research Article

www.acsami.org

Nano- and Macroscale Structural and Mechanical Properties of in Situ Synthesized Bacterial Cellulose/PEO-*b*-PPO-*b*-PEO Biocomposites

Agnieszka Tercjak,*[,†] Junkal Gutierrez,[†] Hernane S. Barud,[‡,§] Rafael R. Domeneguetti,[‡] and Sidney J. L. Ribeiro[‡]

[†]Group 'Materials + Technologies' (GMT), Department of Chemical and Environmental Engineering, Polytechnic School, University of the Basque Country (UPV/EHU), Plaza Europa 1, 20018 Donostia-SanSebastián, Spain

[‡]Laboratory of Photonic Materials, Institute of Chemistry, São Paulo State University - UNESP, Araraquara, 14800-901 Sao Paolo, Brazil

[§]Laboratório de Química Medicinal e Medicina Regenerativa (QUIMMERA), Centro Universitário de Araraquara, Araraquara, 14801-340 Sao Paolo, Brazil

ABSTRACT: Highly transparent biocomposite based on bacterial cellulose (BC) mat modified with poly(ethylene oxide-*b*-propylene oxide-*b*-ethylene oxide) block copolymer (EPE) were fabricated in situ during biosynthesis of bacterial cellulose in a static culture from *Gluconacetobacter xylinum*. The effect of the addition to the culture medium of water-soluble EPE block copolymer on structure, morphology, crystallinity, and final properties of the novel biocomposites was investigated at nano- and macroscale. High compatibility between components was confirmed by ATR-FTIR indicating hydrogen bond formation between the OH group of BC and the PEO block of EPE block copolymer. Structural properties of EPE/BC biocomposites showed a strong effect of EPE block copolymer on the morphology of the BC mats. Thus, the increase of the EPE block copolymer content lead to the generation of spherulites of PEO block, clearly visualized using AFM and MO technique, changing crystallinity of the final EPE/BC biocomposites investigated by XRD. Generally, EPE/BC biocomposites maintain thermal stability and mechanical properties of the BC mat being 1 wt % EPE/BC biocomposite material with the best properties. Biosynthesis of EPE/BC composites open new strategy to the utilization of water-soluble block copolymers in the preparation of BC mat based biocomposites with tunable properties.

KEYWORDS: *bacterial cellulose, block copolymer, biocomposites, atomic force microscopy, mechanical properties*

1. INTRODUCTION

Bacterial cellulose (BC), as a renewable natural nanomaterial, has been used in many fields of application from tissue engineering to the electronics industry, passing through medicine, food packaging, and cosmetics, among others.[1−9] Wide ranging applications of BC are strongly related to its very good mechanical properties, porosity, high crystallinity, high water absorption capability, and good chemical stability, as well as biodegradability and remarkable biocompatibility of this fascinating tridimensional nanofiber network.[1−11]

This naturally nanosized material with a unique porous network structure consists of a self-assembled structure of hierarchically ordered cellulose nanofibers of 3−8 nm in diameter.[12,13] BC can be produced on the large scale using a species of bacteria *Gluconacetobacter* leading to nondrying bacterial cellulose membranes with high water content up to 99%.[8,12,14]

With these features taken into account, it turns out that BC is a potential candidate for use as a matrix for in situ fabrication of biocomposites with both water-soluble polymeric materials[13−22] and inorganic nanoparticles.[23−25] The biosynthesis allows design of novel biocomposites with tunable properties by a one-step pathway and creates biocomposites merging the outstanding properties of bacterial cellulose with the interesting physicochemical properties of polymeric materials or optical,

Received: November 25, 2014
Accepted: January 29, 2015
Published: January 29, 2015

DOI: 10.1021/am508273x
ACS Appl. Mater. Interfaces 2015, 7, 4142−4150

Scheme 1. Schematic Representation of Sample Preparation

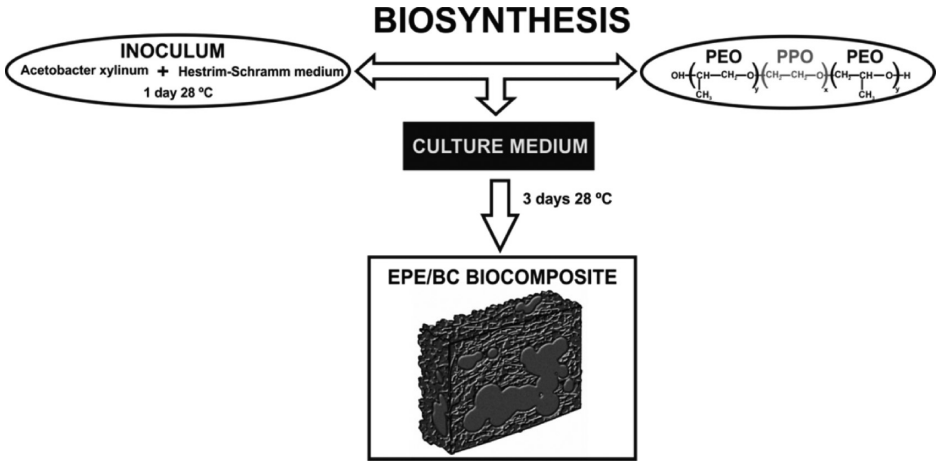

electrical, magnetic, or antibacterial properties of inorganic nanoparticles.

Different biodegradable water-soluble thermoplastics such as poly(ethylene oxide) (PEO),[15,16] poly(vinyl alcohol) (PVA),[17,18] or natural biopolymers such as chitosan,[21] gelatin,[22] aloe vera,[20] or starch[13] were used to design novel multifunctional biocomposites fabricated during biosynthesis of the bacterial cellulose to reach a new range of applications in tissue engineering, wound dressing, food packaging, or electronic field.

However, to the best of our knowledge block copolymers (BCP) have never been used to generate BC-based biocomposites by the in situ fabrication protocol. From this point of view, biocompatible, water-soluble, amphiphilic poly(ethylene oxide-*b*-propylene oxide-*b*-ethylene oxide) block copolymer with a wide range of applications in medicine[26−33] presents a challenge to develop novel biocomposites that link together the abundant properties of the bacterial cellulose membrane with properties offered by the poly(ethylene oxide-*b*-propylene oxide-*b*-ethylene oxide) block copolymer.

With the increasing interest in the study of properties of novel designed biocomposites, not only at macro-, but also at the nanoscale level taken into account, PeakForce quantitative nanomechanical mapping (PeakForce QNM) seems to be the ideal, relatively new imaging mode of the atomic force microscopy (AFM)[34−37] technique used in this approach. This technique allows the determination of mechanical properties of materials such as elastic modulus, adhesion, deformation, and others with nanometer-scale resolution. Consequently, this new AFM imaging mode is a novel methodology and offers a better understanding between the structural and mechanical properties of materials.

In the present work, bacterial cellulose based biocomposites modified with different EPE block copolymer contents were biosynthesized and characterized. AFM in both tapping and PeakForce quantitative nanomechanical mapping (PeakForce QNM) modes was used to study the effect of the addition of EPE block copolymer on the structural and nanomechanical properties of designed EPE/BC biocomposites compared with neat BC mat. Moreover, properties of these EPE/BC biocomposites at the nanoscale level were compared with macroscale properties using an optical microscopy and a tensile testing machine (MTS).

2. MATERIALS AND METHODS

2.1. Production of Inoculum. The strain used was *Gluconacetobacter xylinum* (ATCC 23760) supplied by André Tosello Foundation, Campinas-SP, Brazil. It was cultured in Hestrim-Schramm medium (HS medium) composed of D-glucose, yeast extract, peptone, disodium hydrogen phosphate (Na_2HPO_4), citric acid, agar, and purified water. Analytical grade chemicals were used as received.

The strain culture medium was sterilized before the bacterial strain inoculation and then was cultivated during 1 day at 28 °C in an air-circulating oven as conditioning chamber. This was used as the inoculum for producing BC and EPE/BC biocomposites.

2.2. Biosynthesis of BC and EPE/BC Biocomposites. BC culture medium was prepared according to a method described previously by De Salvi et al.[38] The control culture medium was similar to HS medium and contains D-glucose, yeast extract, magnesium sulfate heptahydrate ($MgSO_4{\cdot}7H_2O$), potassium phosphate monobasic (KH_2PO_4), ethanol, and purified water. Analytical grade chemicals were used as received.

In order to develop EPE/BC biocomposites, different amounts of poly(ethylene oxide-*b*-propylene oxide-*b*-ethylene oxide) (EPE) triblock copolymer purchased from Sigma-Aldrich (Mn 5800 g/mol and 30 wt % of poly(ethylene oxide)) were incorporated in the culture medium of BC. Thus, 0.5, 1, 1.5, and 3 wt % concentrations of EPE block copolymer were added to a 250 mL Erlenmeyer flask containing 45 mL of BC culture medium and then 5 mL of the inoculum was also incorporated. After 3 days of cultivation in static conditions at 28 °C in an air circulating oven, generated jelly-like membranes were removed.

Subsequently, BC membrane and EPE/BC biocomposite membranes were harvested and purified to eliminate the culture medium and byproducts. The purification protocol starts from an immersion in running water for 3 days. Then, membranes were placed in purified water and were heated at 80 °C for 50 min. The same step was repeated, replacing water for a 0.1 M solution of NaOH. Finally, membranes were washed with purified water several times until pH 7.

The schematic representation of the preparation method is show in Scheme 1.

2.3. Characterization Techniques. The optical properties of BC and their biocomposites modified with different EPE block copolymer contents were studied using a UV-3600, Shimadzu UV−vis-NIR Spectrophotometer in the wavelength interval between 200 and 800 nm. The average thickness of the samples used for this measurement was 0.013 ± 0.002 μm.

Fourier transform infrared spectroscopy (FTIR) was used to verify hydrogen bond interactions in EPE/BC biocomposites. Infrared spectra were carried out in a Nicolet Nexus Spectra equipped with a Golden Gate single reflection diamond ATR accessory and were taken with a 2 cm^{-1} resolution in a wavenumber range from 4000 to 400 cm^{-1}.

DOI: 10.1021/am508273x
ACS Appl. Mater. Interfaces 2015, 7, 4142−4150

Thermogravimetric analysis (TGA) was performed using TGA/SDTA-851e equipment under air atmosphere at a heating rate 10 °C min^{-1} from room temperature to 700 °C.

X-ray diffraction (XRD) was carried out on a Philips PW 1710 diffractometer. The Cu Kα X-ray source was set to 40 kV and 100 mA and the samples were examined at room temperature over the angular range of 10° to 30°.

Structural characterization of neat BC mat and their biocomposites with EPE block copolymer was performed using atomic force microscopy (AFM). Corresponding AFM images were obtained by operating in tapping mode with a scanning probe microscope Dimension ICON from Bruker equipped with an integrated silicon tip/cantilever having a resonance frequency of 300 kHz. Scan rates ranged from 0.7 to 1.2 Hz s^{-1}. In order to obtain repeatable results, different regions of the specimens were scanned to choose representative AFM images. With the similarity between height and phase AFM images taken into account, only AFM phase images are shown here. PeakForce quantitative nanomechanical property mapping (PeakForce QNM) was used to study nanomechanical properties of neat BC mat and EPE/BC biocomposites using the same Dimension Icon microscope from Bruker. Measurements were carried out in PeakForce mode under ambient conditions. A silicon tip with nominal radius of 10 nm, cantilever length of 125 μm, and resonance frequency of 150 kHz was used. The measurements were performed with a calibrated optical sensitivity. The exact spring constant of the tip was calculated using the Thermal Tune option and a defined tip radius was adjusted using PS as standard.

The surface homogeneity of investigated neat BC mat and their EPE/BC biocomposites at the macroscale was investigated using an optical microscope (OM) (Nikon Eclipse E600). The investigated materials were analyzed in reflection mode and crossed polarizers were employed to visualize both nucleation and spherulites in the investigated samples. Micrographs were captured with a Color View 12 camera and analyzed using the AnalySIS Auto 3.2 software (Soft Imaging System GmbH).

Mechanical properties at the macroscale level of neat BC mat and designed EPE/BC biocomposites were investigated at room temperature on a tensile testing machine MTS Insight 10 equipment with load cell of 250 N. Specimens of 20 mm length and 5 mm width were tested with strain rate of 1 mm/min. All samples were conditioned for 48 h under vacuum prior to testing. Elongation at break and tensile strength were calculated as average of five test specimen data.

3. RESULTS AND DISCUSSION

Optical properties were studied employing UV−vis spectroscopy. Figure 1 shows UV−vis spectra of neat BC mat and their biocomposites with different EPE block copolymer content. Additionally, visual transparency of all investigated samples is shown as inset in Figure 1. The transparency of EPE/BC biocomposites increased gradually with increasing EPE block copolymer content up to 1.5 wt %. For the EPE block copolymer content higher than 3 wt %, the loss of transparency was detected due to the semicrystalline character of EPE block copolymer uniformly located on the fibers of the BC mat, which will be discussed in more detail using OM results.

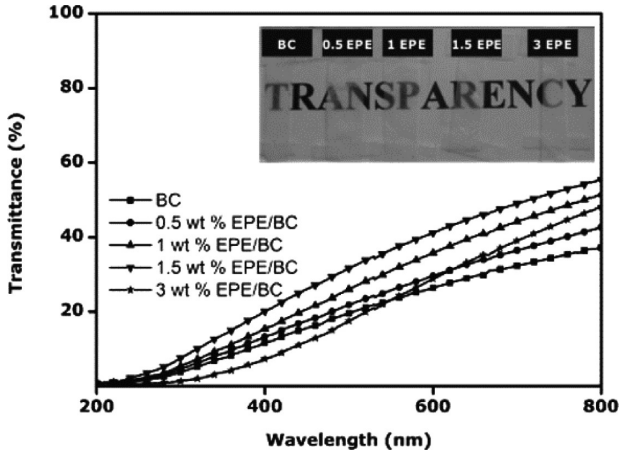

Figure 1. UV−vis transmittance spectra of neat BC mat and designed EPE/BC biocomposites with different EPE block copolymer content (the inset show a digital image of investigated materials).

The transparency of investigated EPE/BC biocomposites was confirmed by their UV−vis transmittance spectra at the visible wavelength range. The transmittance, taken at wavelength equal to 800 nm, increased from 37% for neat BC mat to 55% for biocomposites with 1.5 wt % EPE block copolymer content. Thus, the addition of EPE block copolymer leads to enhancement of the transparency of the neat BC mat.

Transparency is an important property for preparations of the full-biocompatible flexible substrate for optoelectronic applications.[39,40] Biocomposite with the highest EPE block copolymer content (3 wt %) shows a decrease of transmittance to 48%. However, this value is still higher if compared with the transmittance of neat BC mat. This phenomenon is probably related to the semicrystalline character of the EPE block copolymer.

ATR-FTIR spectra of neat BC mat, EPE block copolymer, and their biocomposites with different EPE block copolymer content are shown in Figure 2.

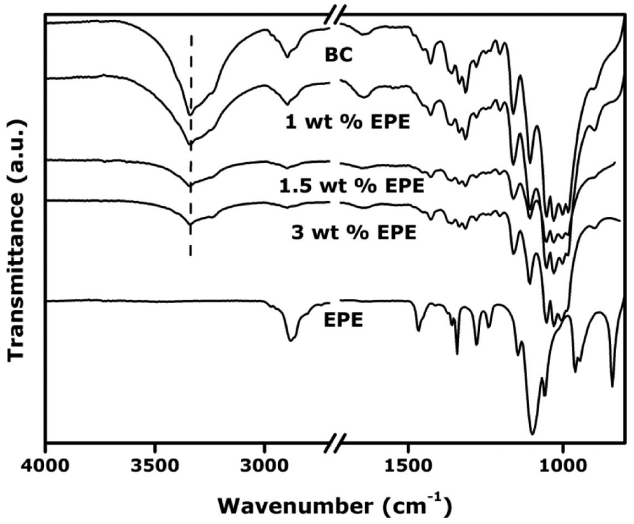

Figure 2. ATR-FTIR spectra of neat BC mat and designed EPE/BC biocomposites with different EPE block copolymer content.

ATR-FTIR spectrum of neat BC mat showed characteristics bands of BC. One can be identified at 3345 cm^{-1} (O−H stretching of cellulose type I), 3240 cm^{-1} (hydrogen bonded O−H), 2895 cm^{-1} (CH stretching of CH_2 groups), 2854 cm^{-1} (CH_2 asymmetric stretching), 1650 cm^{-1} (bending motion of absorbed water H−O−H), 1427 cm^{-1} (CH_2 symmetric bending), 1365 cm^{-1} (CH bending), 1160 cm^{-1} (C−O−C asymmetric stretching), and 1060 cm^{-1} (C−O stretching).[41−43] As expected, ATR-FTIR spectra of neat EPE block copolymer displayed a characteristic band at 1098 cm^{-1} related to the stretching vibration of the C−O−C group of the ether bonding and at 1462 cm^{-1} assigned to the C−H bending vibration.

DOI: 10.1021/am508273x
ACS Appl. Mater. Interfaces 2015, 7, 4142−4150

Similarly to ATR-FTIR spectrum of neat BC mat, ATR-FTIR spectra of the EPE/BC biocomposites showed a typical −OH stretching band, which shifts to higher wavenumbers if compared to the wavenumber for analogical vibration of BC: being 3348 cm^{-1} for 0.5 wt % EPE/BC biocomposite and 3352 cm^{-1} for 3 wt % EPE/BC biocomposite. Moreover, ATR-FTIR spectra of the EPE/BC biocomposites do not show the formation of any additional bands if compared with ATR-FTIR spectra of neat BC mat and neat EPE block copolymer, which confirm lack of chemical bonds between components of EPE/BC biocomposites. However, the strong hydrogen bonds between −OH groups of the neat BC mat and neat PEO block of EPE block copolymer were confirmed by considerable variation in stretching vibration of the hydrogen bonds in ATR-FTIR spectra of EPE/BC biocomposites if compared with ATR-FTIR spectrum of neat BC mat.

With the aim of determining the decomposition temperature of the EPE/BC biocomposites, thermogravimetric curves of neat EPE block copolymer, neat BC mat, and corresponding biocomposites are shown in Figure 3. As can be clearly observed, EPE block copolymer showed only a one-step decomposition process with the decomposition temperature at 250 °C. Under the same measurement conditions, the TGA curve corresponding to neat BC mat showed two typical decomposition steps located at approximately 350 and 460 °C.[44]

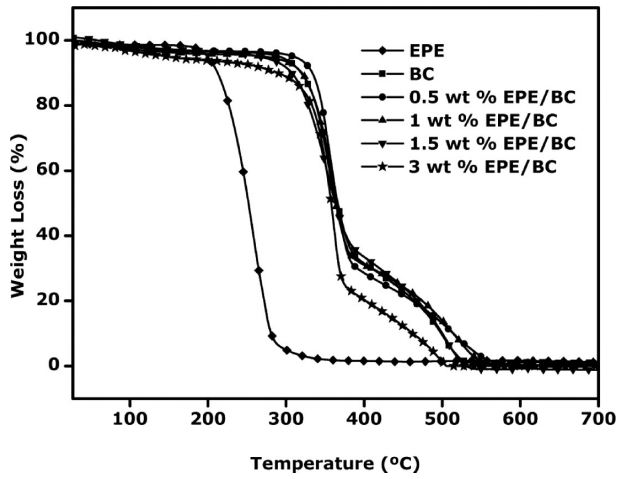

Figure 3. Thermogravimetric curves of neat BC mat, neat EPE block copolymer, and designed EPE/BC biocomposites with different EPE block copolymer content.

As visualized in Figure 3, EPE/BC biocomposites followed the decomposition process similar to that of neat BC. Thus, TGA curves of EPE/BC biocomposites clearly indicated that even addition of 3 wt % EPE block copolymer does not significantly change the decomposition process of biocomposites if compared with decomposition of neat BC mat. Addition of 0.5 wt % of EPE block copolymer shifted the decomposition temperatures to 354 and 455 °C for the first and second decomposition steps, respectively. The addition of 3 wt % shifted the decomposition temperature to 345 and 440 °C compared with the temperature of first and second decomposition steps for neat BC mat. This sharp decrease to lower temperatures can be attributed to high compatibility between EPE block copolymer and BC probably related to the formation of hydrogen bond between −OH groups of BC and PEO-block of EPE block copolymer. This fact is in with good agreement with ATR-FTIR results of investigated biocomposites. Similar thermal decomposition behavior was observed for biocomposites based on BC modified with PEO[16] and PVA.[18]

The semicrystalline nature of neat components and EPE/BC biocomposites were studied using X-ray diffraction. The X-ray diffractograms of neat BC mat, EPE block copolymer, and their biocomposites are plotted in Figure 4.

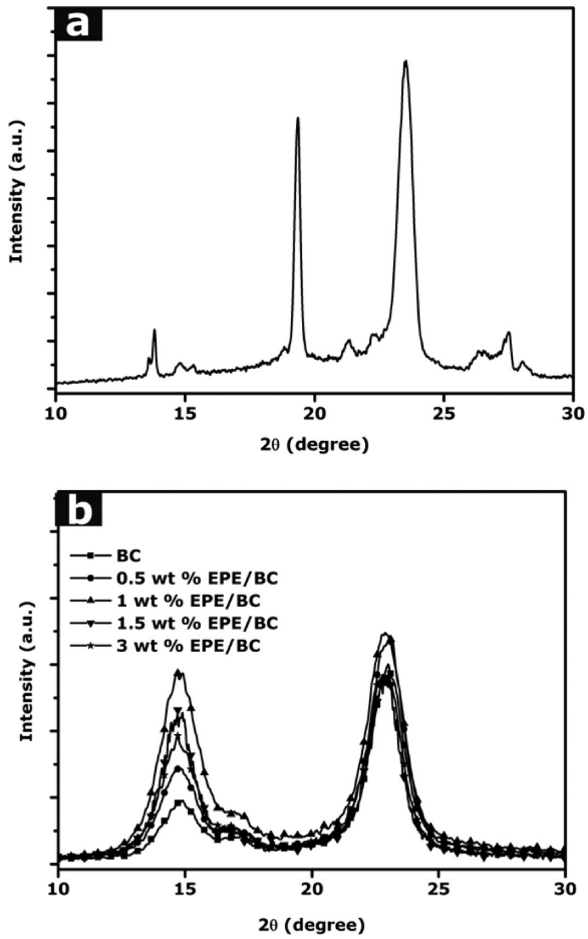

Figure 4. X-ray diffraction of (a) neat EPE block copolymer and (b) neat BC mat and designed EPE/BC biocomposites with different EPE block copolymer content.

XRD pattern of neat BC mat showed three characteristic peaks clearly distinguished at 2θ of approximately 14.9°, 17.2°, and 23° which correspond, as reported in the literature,[44−46] to the primary diffraction of the (101), (101), and (002) polymorphism cellulose I. Regarding the XRD pattern of neat EPE block copolymer, two strong crystalline peaks were observed at 2θ = 19.3° and 23.5°. As can be clearly observed in Figure 4, the X-ray diffractograms of EPE/BC biocomposites are similar to those of neat BC mat with peaks almost in the same 2θ region confirming that BC maintains polymorphism of cellulose I in designed biocomposites. The changes in the peak intensity at 2θ of ∼14.9° suggested strong influence of addition of EPE block copolymer. The relative crystallinity calculated using equations proposed by Segal et al.[47] indicates slight increase of the crystallinity being around 77% for neat BC mat and between 79% and 82% for EPE/BC biocomposites. This insignificant increase in relative crystallinity can be related, on

DOI: 10.1021/am508273x
ACS Appl. Mater. Interfaces 2015, 7, 4142−4150

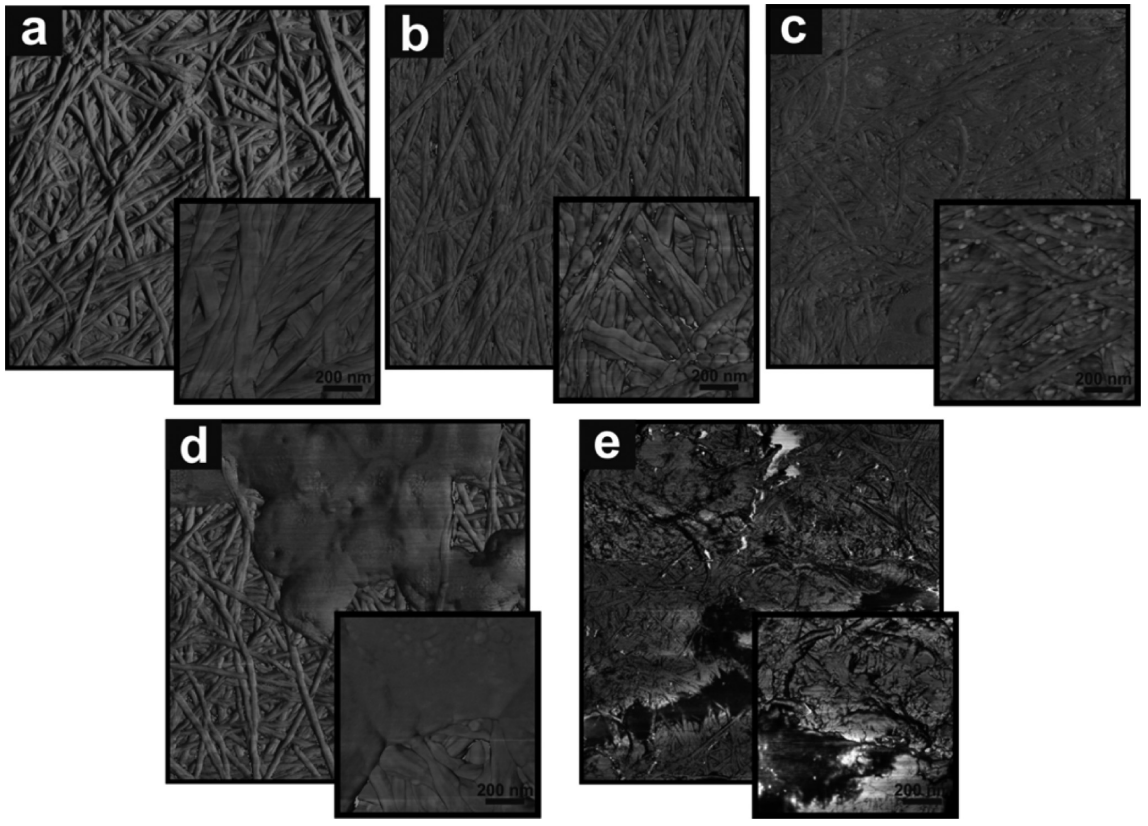

Figure 5. AFM phase images (5 μm × 5 μm) of (a) of neat BC mat and EPE/BC biocomposites containing (b) 0.5 wt %, (c) 1 wt %, (d) 1.5 wt %, and (e) 3 wt % EPE block copolymer. The insets correspond to higher magnification images.

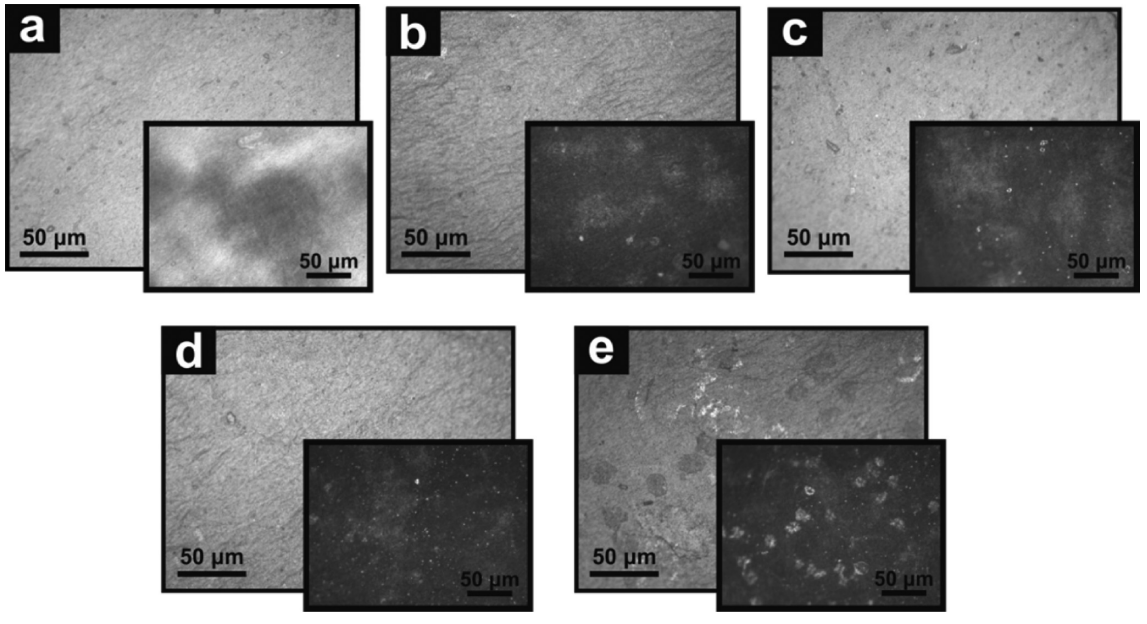

Figure 6. OM micrographs of (a) neat BC mat and designed EPE/BC biocomposites containing (b) 0.5 wt %, (c) 1 wt %, (d) 1.5 wt %, and (e) 3 wt % EPE block copolymer. The insets correspond to the same analyzed area between crossed polarizers.

one hand, to the fact that the PEO block of EPE block copolymer can act as nucleation agent for the crystallization of BC mat, and on the other hand, some part of the crystalline phase of the PEO block of EPE block copolymer can crystallize within the BC mat.

Figure 5 shows AFM phase images of the surface of neat BC mat and EPE/BC biocomposites recorded to study the structural properties of investigated materials.

As is well-known from literature, neat BC mat was constituted of a highly interconnected network of nanofibers with porous tridimensional structure as can be easily recognized in Figure 5a. The diameter of these nanofibers was in the range

DOI: 10.1021/am508273x
ACS Appl. Mater. Interfaces 2015, 7, 4142−4150

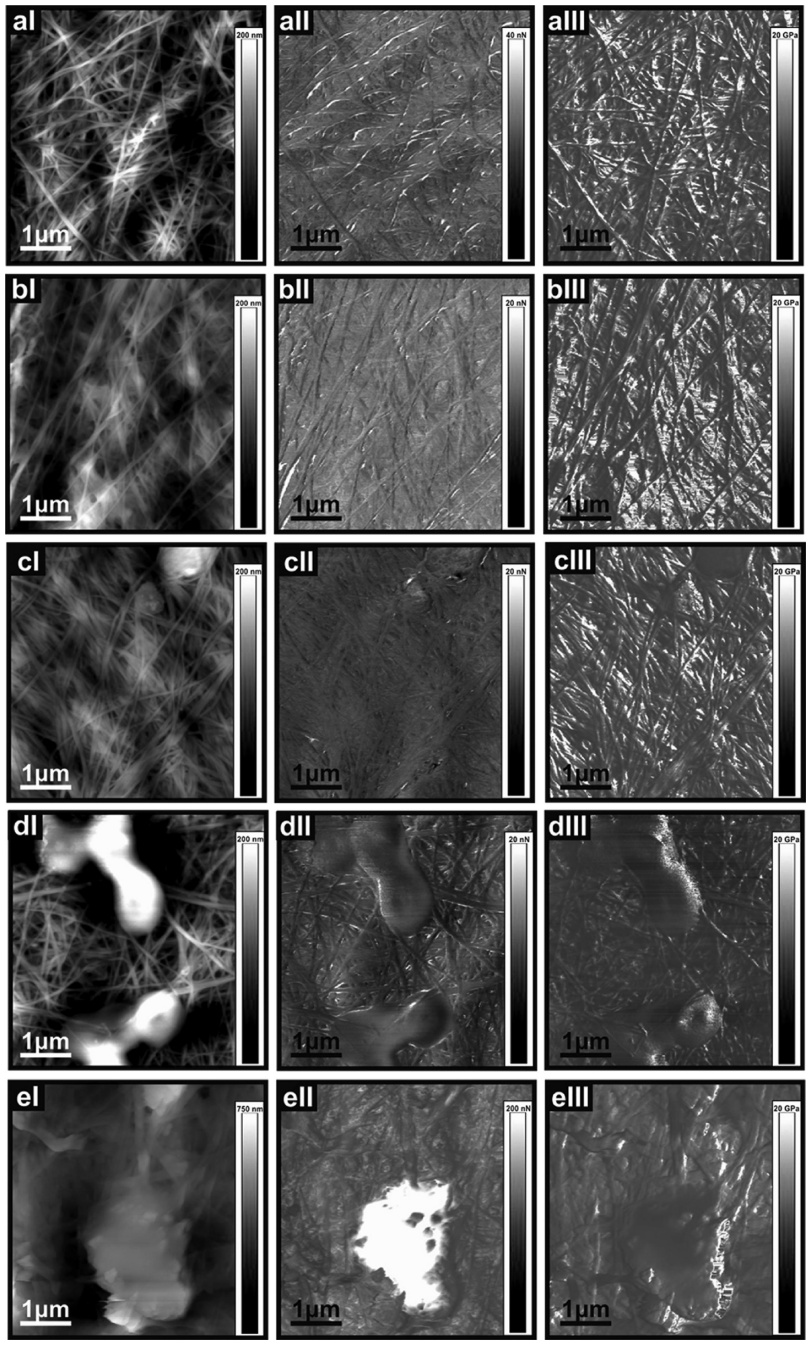

Figure 7. PeakForce QNM images (5 μm × 5 μm) of neat BC mat: (aI) height, (aII) adhesion, (aIII) modulus; and designed EPE/BC biocomposites containing: 0.5 wt % (bI) height, (bII) adhesion, (bIII) modulus; 1 wt % (cI) height, (cII) adhesion, (cIII) modulus; 1.5 wt % (dI) height, (dII) adhesion, (dIII) modulus; 3 wt % (eI) height, (eII) adhesion, (eIII) modulus.

of 25−100 nm as visualized in the inset of Figure 5a. Many of these nanofibers consist of 3−4 fibrils, which were twisted together forming braids. As clearly seen in corresponding AFM phase images, EPE/BC biocomposites preserve the hierarchically ordered tridimensional network structure of the BC mat. Introduction of 0.5 wt % of EPE block copolymer does not significantly affect the BC tridimensional nanometric network structure. The diameter of the nanofibers in 0.5 wt % EPE/BC biocomposite is in the same range as for neat BC mat. Similarly, the addition of 1, 1.5, and 3 wt % does not significantly affect the tridimensional bacterial cellulose network formation; however, as seen in Figure 5c the presence of 1 wt % of EPE block copolymer is enough to visualize homogeneously dispersed, nanometric in size EPE block copolymer domains located on the surface of the BC nanofibers: 25−50 nm in size. The good dispersion of EPE block copolymer can be related to the intermolecular hydrogen bond interaction confirmed by the ATR-FTIR technique.

In the case of EPE/BC biocomposites with EPE block copolymer content higher than 1.5 wt %, one can easily observe that the thermoplastic block copolymer domains cover different regions of the BC mat, and a larger area is covered with the increase of the EPE block copolymer content. Similar behavior was observed by Pircher et al.[48] for bacterial cellulose aerogels modified with poly(lactic acid) (PLA).

DOI: 10.1021/am508273x
ACS Appl. Mater. Interfaces 2015, 7, 4142−4150

Here, it should be pointed out that addition of even 3 wt % of EPE block copolymer leads to a biocomposite which is still able to form a 3D network, interconnected nanofiber structure during BC growth, thus confirming, in this way, high compatibility and high integration of EPE block copolymer with BC. Compact, highly integrated biomaterials can design addition of EPE block copolymers, which does not affect the network formation process of the BC mat.

OM micrographs taken for neat BC mat and EPE/BC biocomposites (Figure 6) confirm that all investigated materials form continuous random network flat surfaces without any defects.

The increase of the EPE block copolymer provokes the crystallization of the PEO block of EPE block copolymer as clearly detected by OM micrographs taken between crossed polarizers (see insets corresponding to each EPE/BC biocomposite). Addition of EPE block copolymer leads to formation of nucleus and spherulites of PEO block of the EPE block copolymer, which appeared as bright areas on the darker crystalline BC. Here it should be pointed out that, under OM measurement, no spherulites for either neat BC mat or BC phase in EPE/BC biocomposites were observed. PEO block spherulites increase with increasing EPE block copolymer content in EPE/BC biocomposites and covered a larger area of the BC mat surface. The OM results obtained are in good agreement with the results obtained by AFM related with the structure of investigated biocomposites at the nanometric scale.

Quantitative nanomechanical properties (QNM) of neat BC mat and EPE/BC biocomposites were studied employing atomic force microscopy in PeakForce mode. This technique allows simultaneously mapping of AFM height, adhesion, and elastic modulus images, which are shown in Figure 7. Here, it should be noted that, by calculation from AFM height images, the average roughness (R_a) of EPE/BC biocomposites increased with increasing EPE block copolymer content, being around 55 nm for neat BC mat, 70 nm for 0.5 wt % EPE/BC biocomposite, and 130 nm for 3 wt % EPE/BC block copolymer. The significant increase of R_a is probably related to the semicrystalline character of the PEO block of EPE block copolymer. As clearly distinguished in AFM height images and as has been described above for AFM phase images, the addition of 1 wt % EPE led to the formation of small nanometric domains of EPE phase, which change to spherical spherulites with 800−900 nm in diameter after the addition 1.5 wt % of EPE block copolymer. Thus, as expected, the formation of tridimensional spherulites of the PEO block of EPE block copolymer on the surface of the BC nanofiber network changed the average roughness of the EPE/BC biocomposites.

Here, it should be pointed out that the R_a of the investigated biocomposites from areas where the tridimensional nanofibers network is not covered by EPE block copolymer is similar to that for neat BC mat, which once more confirmed that EPE/BC biocomposites do not lose the 3D network structure created during BC growth.

The AFM adhesion and elastic modulus images of neat BC mat revealed the existence of two areas with different adhesion force (one with adhesion force ∼5 nN and the other one ∼15 nN) and elastic modulus (one ∼2−4 GPa and the other one ∼20−23 GPa), both uniformly distributed on the entire investigated surface. As is well-known, the crystalline phases of polymers have higher mechanical properties if compared to the amorphous phase. Consequently, PeakForce QNM measurement of neat BC mat allowed us to clearly distinguish higher local elastic modulus, which corresponds to crystalline phase of BC mat, and lower modulus, corresponding to amorphous phase of BC mat. Additionally, here it should be pointed out that the average elastic modulus corresponding to a 5 μm × 5 μm mapped area was 4.2 GPa. PeakForce QNM properties of 0.5 wt % EPE/BC biocomposite showed mechanical properties very similar to those for neat BC mat, with average elastic modulus equal to 4 GPa. Addition of a higher amount of EPE block copolymer leads to a decrease of the average elastic modulus to 3.6 GPa for 1 wt % EPE/BC biocomposite, 2.4 GPa for 1.5 wt % EPE/BC biocomposite, and 1.7 GPa for 3 wt % EPE/BC biocomposite. This can be related to the plasticizing effect of the softer EPE block copolymer when compared to the BC nanofibers. As expected, the elastic modulus of the EPE block copolymer phase was lower than 1 GPa and the adhesion forces were much greater, 160−180 nN for 3 wt % EPE/BC biocomposite.

Macroscale mechanical properties of neat BC mat and designed EPE/BC biocomposites are graphed on Figure 8. Under the same testing conditions, the elongation at break increased with increasing EPE block copolymer content up to 1 wt % in comparison to the elongation at break of neat BC mat. The addition of more than 1.5 wt % EPE block copolymer

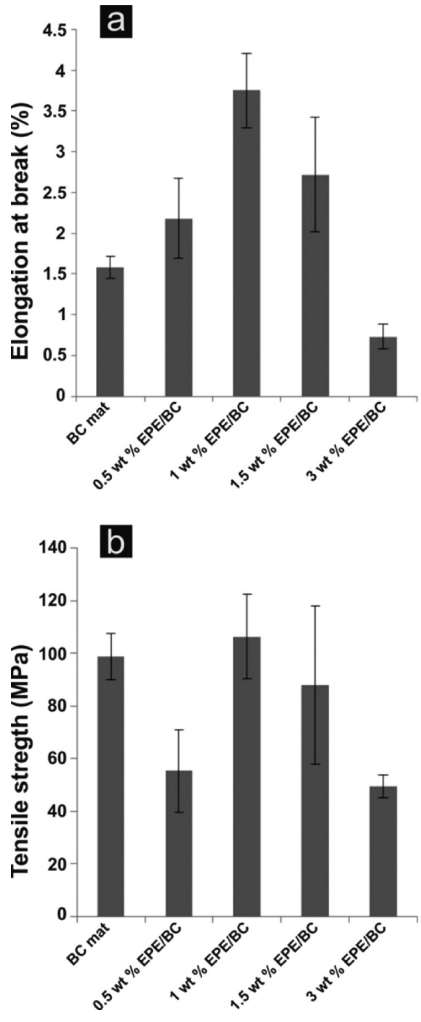

Figure 8. (a) Elongation at break and (b) tensile strain of neat BC mat and designed EPE/BC biocomposites with different EPE block copolymer content.

DOI: 10.1021/am508273x
ACS Appl. Mater. Interfaces 2015, 7, 4142−4150

provoked a decrease of elongation at break. Results confirm good adhesion between bacterial cellulose and EPE block copolymer up to 1 wt % of EPE block copolymer content. On the contrary, for EPE/BC biocomposites with EPE block copolymer content above 1 wt %, the adhesion between components decreased.

This behavior can be related to the fact that addition of up to 1 wt % of EPE block copolymer results in a slight increase of crystallinity of the bacterial cellulose phase (confirmed by XRD) and formation of small nanometric nucleus of PEO block of EPE block copolymer (confirmed by AFM) leading to well-integrated biocomposites with uniform nanometric distribution of EPE block copolymer. Consequently, the higher elongation at break can be attributed to the restrained chain movement and refined crystalline structure during the deformation. Addition of more than 1.5 wt % provoked crystallization of the PEO block of the EPE block copolymer at macroscale (OM results) changing adhesion between the components.

Simultaneously, as can be observed in Figure 8, the general tendency of the tensile strain at macroscale is similar if compared with results obtained at the nanoscale level using atomic force microscopy in PeakForce mode (except 0.5 wt % EPE block copolymer, which can be simply related to the natural character of the in situ fabricated biocomposites).

In the case of designed EPE/BC biocomposites, tensile strain slightly decreased if compared with neat BC mat. This behavior can be related to the formation of strong intramolecular hydrogen bonds between PEO block of EPE block copolymer and −OH bonds of BC located on the nanofiber surface.

On the contrary, in the case of 3 wt % EPE/BC biocomposite the presence of spherulites of the PEO block of EPE block copolymer provokes the weakness of the intramolecular hydrogen bonds resulting in a decrease of the compatibility between both components.[12]

Consequently, as can be clearly observed in Figure 8b, the tensile strain of this EPE/BC biocomposite slightly decreased in comparison with the tensile strain of neat BC mat, ∼50 MPa for 3 wt % EPE/BC biocomposite. The best mechanical properties at macroscale were achieved for 1 wt % EPE/BC biocomposite.

4. CONCLUSIONS

Biocomposites based on BC mat modified with different biocompatible, amphiphilic EPE block copolymer contents were prepared in situ during bioengineering production of BC mat from *Gluconacetobacter xylinum* in static conditions. As expected, the formation of intermolecular hydrogen bonds between −OH groups on the surface of the BC nanofibers and PEO block of the EPE block copolymer was confirmed by ATR-FTIR results. Thermal behavior of designed BC/EPE biocomposites indicated that the thermal stability of the neat BC mat was maintained, which proves the strong compatibility between both components. UV−vis transmittance spectra of BC/EPE biocomposites confirmed higher transparency of designed materials compared to the transparency of neat BC mat.

Nanoscale structural and mechanical properties of EPE/BC biocomposites were studied employing AFM and PeakForce quantitative nanomechanical mapping and analogous macroscale properties using OM and tensile testing machines. The addition of EPE block copolymer has a strong influence on the final structural and mechanical properties of EPE/BC biocomposites.

Novel highly transparent EPE/BC biocomposites lead to the development of materials which linked together good mechanical properties of BC mat with properties offered by EPE block copolymer.

AUTHOR INFORMATION

Corresponding Author

*E-mail address: agnieszka.tercjaks@ehu.eus. Tel.: +34 943 017 163; Fax: +34 943 017 130.

Notes

The authors declare no competing financial interest.

ACKNOWLEDGMENTS

This work was supported by Brazilian agencies CNPq, FAPESP, and CAPES. Financial support from the Basque Country Government in the frame of Grupos Consolidados (IT-776-13) and from MINECO in the frame of DECAION (MAT2012-31675) are gratefully acknowledged. J. G. acknowledges the UPV/EHU for Postdoctoral Fellow (ESDOC13/059), A.T. acknowledges MICINN for the Ramón y Cajal program (RYC-2010-05592). Moreover, we are grateful to the 'Macrobehavior-Mesostructure-Nanotechnology' SGIker unit of the UPV/EHU.

REFERENCES

(1) Hoenich, N. Cellulose for Medical Applications: Past, Present, and Future. *Bioresources* **2006**, *1*, 270−280.
(2) Klemm, D.; Schumann, D.; Udhardt, U.; Marsch, S. Bacterial Synthesized Cellulose-Artifical Blood Vessels for Microsurgery. *Prog. Polym. Sci.* **2001**, *26*, 1561−1603.
(3) Zhu, H.; Fang, Z.; Preston, C.; Li, Y.; Hu, L. Transparent Paper: Fabrications, Properties, and Device Applications. *Energy Environ. Sci.* **2014**, *7*, 269−287.
(4) Qiu, K.; Netravali, A. N. Review of Fabrication and Applications of Bacterial Cellulose Based Nanocomposites. *Polym. Rev.* **2014**, *54*, 598−626.
(5) Hu, W.; Chen, S.; Yang, J.; Li, Z.; Wang, H. Functionalized Bacterial Cellulose Derivatives and Nanocomposites. *Carbohydr. Polym.* **2014**, *101*, 1043−1060.
(6) Shi, Z.; Zhang, Y.; Phillips, G. O.; Yang, G. Utilization of Bacterial Cellulose in Food. *Food Hydrocoll.* **2014**, *35*, 539−545.
(7) Lin, W. Ch.; Lien, Ch. Ch.; Yeh, H. J.; Yu, Ch. M.; Hsu, S. H. Bacterial Cellulose And Bacterial Cellulose−Chitosan Membranes for Wound Dressing Applications. *Carbohydr. Polym.* **2013**, *94*, 603−611.
(8) Lin, S. P.; Calvar, I. L.; Catchmark, J. M.; Liu, J. R.; Demirci, A.; Cheng, K. Biosynthesis, Production and Applications of Bacterial Cellulose. *Cellulose* **2013**, *20*, 2191−2219.
(9) Fua, L.; Zhanga, J.; Yanga, G. Present Status and Applications of Bacterial Cellulose-Based Materials for Skin Tissue Repair. *Carbohydr. Polym.* **2013**, *92*, 1432−1442.
(10) Hsieh, Y. C.; Yano, H.; Nogi, M.; Eichhorn, S. J. An Estimation of the Young's Modulus of Bacterial Cellulose Filaments. *Cellulose* **2008**, *15*, 507−513.
(11) Yano, H.; Sugiyama, J.; Nakagaito, A. N.; Nogi, M.; Matsuura, T.; Hikita, M.; Handa, K. Optically Transparent Composites Reinforced with Networks of Bacterial Nanofibers. *Adv. Mater.* **2005**, *17*, 153−155.
(12) Iguchi, M.; Yamanaka, S.; Budhiono, A. Bacterial Cellulose-A Masterpiece of Nature's Arts. *J. Mater. Sci.* **2000**, *35*, 261−270.
(13) Grande, C. J.; Torres, F. G.; Gomez, C. M.; Troncoso, O. P.; Canet-Ferrer, J.; Martínez-Pastor, J. Development of Self-Assembled Bacterial Cellulose-Starch Nanocomposites. *Mater. Sci. Eng., C* **2009**, *29*, 1098−1104.
(14) Seifert, M.; Hesse, S.; Karbelian, V.; Klemm, D. Controlling the Water Content Of Never Dried and Reswollen Bacterial Cellulose By

DOI: 10.1021/am508273x
ACS Appl. Mater. Interfaces 2015, 7, 4142−4150

The Addition Of Water-Soluble Polymers To The Culture Medium. *J. Polym. Sci., Part A: Polym. Chem.* **2004**, *42*, 463−470.
(15) Heßler, N.; Klemm, D. Alteration of Bacterial Nanocellulose Structure by in situ Modification Using Polyethylene Glycol and Carbohydrate Additives. *Cellulose* **2009**, *16*, 899−910.
(16) Brown, E. E.; Laborie, M. P. G. Bioengineering Bacterial Cellulose/Poly(Ethylene Oxide) Nanocomposites. *Biomacromolecules* **2007**, *8*, 3074−3081.
(17) Gea, S.; Bilotti, E.; Reynolds, C. T.; Soykeabkeaw, N.; Peijs, T. Bacterial Cellulose−Poly(Vinyl Alcohol) Nanocomposites Prepared by an in-Situ Process. *Mater. Lett.* **2010**, *64*, 901−904.
(18) Castro, C.; Vesterinen, A.; Zuluaga, R.; Caro, G.; Filpponen, I.; Rojas, O. J.; Kortaberria, G.; Gañan, P. In Situ Production of Nanocomposites of Poly(Vinyl Alcohol) and Cellulose Nanofibrils from Gluconacetobacter Bacteria, Effect of Chemical Crosslinking. *Cellulose* **2014**, *21*, 1745−1756.
(19) Brown, E. E.; Zhang, J.; Laborie, M. P. G. Never-Dried Bacterial Cellulose/Fibrin Composites, Preparation. Morphology and Mechanical Properties. *Cellulose* **2011**, *18*, 631−641.
(20) Saibuatong, O.; Phisalaphong, M. Novo Aloe Vera-Bacterial Cellulose Composite Film from Biosynthesis. *Carbohydr. Polym.* **2010**, *79*, 455−460.
(21) Phisalaphong, M.; Jatupaiboon, N. Biosynthesis and Characterization Of Bacteria Cellulose−Chitosan Film. *Carbohydr. Polym.* **2008**, *74*, 482−488.
(22) Taokaew, S.; Seetabhawang, S.; Siripong, P.; Phisalaphong, M. Biosynthesis and Characterization of Nanocellulose-Gelatin Films. *Materials* **2013**, *6*, 782−794.
(23) Jian, J.; Zheng, Y.; Song, W.; Luan, J.; Wen, X.; Wu, Z.; Chen, X.; Wang, Q.; Guo, S. In Situ Synthesis of Silver-Nanoparticles/Bacterial Cellulose Composites for Slow-Released Antimicrobial Wound Dressing. *Carbohydr. Polym.* **2014**, *102*, 762−771.
(24) Li, X.; Chen, S.; Hu, W.; Shi, S.; Shen, W.; Zhang, X.; Wang, H. In Situ Synthesis of CdS Nanoparticles on Bacterial Cellulose Nanofibers. *Carbohydr. Polym.* **2009**, *76*, 509−512.
(25) Liu, Ch.; Yang, D.; Wang, Y.; Shi, J.; Jiang, Z. Fabrication of Antimicrobial Bacterial Cellulose-Ag/AgCl Nanocomposite Using Bacteria as Versatile Biofactory. *J. Nanopart. Res.* **2012**, *14*, 1084−1089.
(26) Marin, A.; Sun, H.; Husseini, G. A.; Pitt, W. G.; Christensena, D. A.; Rapoport, N. Y. Drug Delivery in Pluronic Micelles, Effect of High-Frequency Ultrasound on Drug Release From Micelles and Intracellular Uptake. *J. Controlled Release* **2002**, *84*, 39−47.
(27) Hamley, I. W. Introduction to Soft Matter. In *Synthetic and Biological Self-Assembling Materials*; Wiley: Chichester, 2000; pp 193−263.
(28) Shachaf, Y.; Gonen-Wadmany, M.; Seliktar, D. The Biocompatibility of Pluronic® F127 Fibrinogen-based Hydrogels. *Biomaterials* **2010**, *31*, 2836−2847.
(29) Zhang, W.; Gilstrap, K.; Wu, L.; Bahadur, K. C. R.; Moss, M. A.; Wang, Q.; Lu, X.; He, X. Synthesis and Characterization of Thermally Responsive PluronicF127 Chitosan Nanocapsules for Controlled Release and Intracellular Delivery of Small Molecules. *ACS Nano* **2010**, *4*, 6747−6759.
(30) Barthel, M. J.; Schacher, F. H.; Schubert, U. S. Poly(ethylene oxide) (PEO)-based ABC Triblock Terpolymers − Synthetic Complexity vs. Application Benefits. *Polym. Chem.* **2014**, *5*, 2647−2662.
(31) Kabanov, A. V.; Lemieux, P.; Vinogradov, S.; Alakhov, V. Pluronic® Block Copolymers, Novel Functional Molecules for Gene Therapy. *Adv. Drug Delivery Rev.* **2002**, *54*, 223−233.
(32) Schmaljohann, D. Thermo- and pH-Responsive Polymers in Drug Delivery. *Adv. Drug Delivery Rev.* **2006**, *58*, 1655−1670.
(33) Van Vlierberghe, S.; Dubruel, P.; Schacht, E. Biopolymer-based Hydrogels as Scaffolds for Tissue Engineering Applications. *Biomacromolecules* **2011**, *12*, 1387−1408.
(34) Panaitescu, D. M.; Frone, A. N.; Nicolae, C. Micro- and Nano-Mechanical Characterization of Polyamide 11 and its Composites Containing Cellulose Nanofibers. *Eur. Polym. J.* **2013**, *49*, 3857−3866.
(35) Sababi, M.; Kettle, J.; Rautkoski, H.; Claesson, P. M.; Thormann, E. Structural and Nanomechanical Properties of Paperboard Coatings Studied by Peak Force Tapping Atomic Force Microscopy. *ACS Appl. Mater. Interfaces* **2012**, *4*, 5534−5541.
(36) Panaitescu, D. M.; Frone, A. N.; Spataru, I. C. Effect of Nanosilica on the Morphology of Polyethylene Investigated by AFM. *Compos. Sci. Technol.* **2013**, *74*, 131−138.
(37) Gutierrez, J.; Mondragon, I.; Tercjak, A. Quantitative Nanoelectrical and Nanomechanical Properties of Nanostructured Hybrid Composites by Peakforce Tunneling Atomic Force Microscopy. *J. Phys. Chem. C* **2014**, *118*, 1206−1212.
(38) De Salvi, D. T. B.; Barud, H. S.; Treu-Filho, O.; Pawlicka, A.; Mattos, R. I.; Raphael, E.; Ribeiro, S. J. L. Preparation, Thermal Characterization, and DFT Study of the Bacterial Cellulose Triethanolamine System. *J. Therm. Anal. Calorim.* **2014**, *118*, 205−215.
(39) Barud, H. S.; Caiut, J. M. A.; Dexpert-Ghys, J.; Messaddeq, Y.; Ribeiro, S. J. L. Transparent Bacterial Cellulose−Boehmite−Epoxi-Siloxane Nanocomposites. *Composites, Part A* **2012**, *43*, 973−977.
(40) Legnani, C.; Vilani, C.; Calil, V. L.; Barud, H. S.; Quirino, W. G.; Achete, C. A.; Ribeiro, S. J. L.; Cremona, M. Bacterial Cellulose Membrane as Flexible Substrate for Organic Light Emitting Devices. *Thin Solid Films* **2008**, *517*, 1016−1020.
(41) Oh, S. Y.; Yoo, D. I.; Shin, V.; Kim, H. C.; Kim, H. Y.; Chung, V. S.; Park, W. H.; Youk, H. Crystalline Structure Analysis of Cellulose Treated with Sodium Hydroxide and Carbon Dioxide by Means of X-ray Diffraction and FTIR Spectroscopy. *Carbohydr. Res.* **2005**, *340*, 2376−2391.
(42) Kondo, T.; Sawatari, C. A Fourier Transform Infrared Spectroscopic Analysis of the Character of Hydrogen Bonds in Amorphous Cellulose. *Polymer* **1996**, *37*, 393−399.
(43) Barud, H. S.; de Assuncão, R. M. N.; Martines, M. A. U.; Ghys, J. D.; Marques, R. F. C.; Messaddeq, Y. Bacterial Cellulose-Silica Organic-Inorganic Hybrids. *J. Sol-Gel Sci. Technol.* **2008**, *46*, 363−367.
(44) Barud, H. S.; Barrios, C.; Regiani, T.; Marques, R. F. C.; Verelst, M.; Dexpert-Ghys, J.; Messaddeq, Y.; Ribeiro, S. J. L. Self-Supported Silver Nanoparticles Containing Bacterial Cellulose Membranes. *Mater. Sci. Eng., C* **2008**, *28*, 515−518.
(45) Czaja, W.; Romanovicz, D.; Brown, R. M. Structural Investigations of Microbial Cellulose Produced in Stationary and Agitated Culture. *Cellulose* **2004**, *11*, 403−411.
(46) Garvey, C. J.; Parker, I. H.; Simon, G. P. On the Interpretation of X-Ray Diffraction Powder Patterns in Terms of the Nanostructure of Cellulose I Fibres. *Macromol. Chem. Phys.* **2005**, *206*, 1568−1575.
(47) Segal, L.; Creely, J. J.; Martin, A. E., Jr.; Conrad, C. M. An Empirical Method for Estimating the Degree of Crystallinity of Native Cellulose Using the X-Ray Diffractometer. *Tex. Res. J.* **1959**, *29*, 786−794.
(48) Pircher, N.; Veigel, S.; Aigner, N.; Nedelec, J. M.; Rosenau, T.; Liebner, F. Reinforcement of Bacterial Cellulose Aerogels with Biocompatible Polymers. *Carbohydr. Polym.* **2014**, *111*, 505−513.
(49) Yu, H. Y.; Qin, Z. Y.; Yan, Ch. F.; Yao, J. M. Green Nanocomposites based on Funcionalized Cellulose Nanocrystals, A Study on the Relationship Between Interfacial Interaction and Property Enhancement. *ACS Sustainable Chem. Eng.* **2014**, *2*, 875−896.

DOI: 10.1021/am508273x
ACS Appl. Mater. Interfaces 2015, 7, 4142−4150